IEEE Open Journal of
Antennas and Propagation

Received 13 January 2023; revised 8 February 2023; accepted 12 February 2023. Date of publication 16 February 2023; date of current version 6 April 2023.

Digital Object Identifier 10.1109/OJAP.2023.3245819

Wideband and Dual-Polarized Crossed Dipole Antenna Design Using Substrate-Integrated Coax

SOUMITRA BISWAS (Senior Member, IEEE)

Envistacom LLC, Peachtree Corners, GA 30092, USA

CORRESPONDING AUTHOR: S. BISWAS (e-mail: biswas@ieee.org)

ABSTRACT A wideband and dual-polarized dipole antenna design technique is presented. The proposed antenna employs two sets of dipole elements in orthogonal configuration and separated by a dielectric layer. The dipole elements are excited with two separate substrate-integrated-coaxial feeds to achieve high port-to-port isolation and the overall antenna stackup is enclosed in a substrate-integrated-waveguide (SIW) cavity. To validate the proposed substrate-integrated-coaxial fed dual-polarized antenna design method, a prototype antenna was fabricated using standard multi-layer printed circuit board (PCB) manufacturing technologies to operate in the Ku-band. Measured and simulated results exhibit that the designed antenna has a wide impedance bandwidth of less than -10dB reflection coefficients at 10.28-14.8GHz and the port-to-port isolation between the two orthogonally polarized dipole antenna ports is greater than 20dB at most frequencies, making it suitable for many applications such as satellite communications. The antenna has a relatively stable gain pattern with a gain value of 5.5-6.5dBi and a low cross-polarization level (lower than 16dB) over the operating frequency range.

INDEX TERMS Dual-polarization, wide bandwidth, high port-to-port isolation, low cross-polarization, substrate-integrated-waveguide (SIW), printed circuit board (PCB) antennas, substrate-integrated coax.

I. INTRODUCTION

With the rapid advances in modern wireless communication systems, the increasing demand for high data rate is becoming a critical issue in many applications such as mobile communications and satellite communications system. The wideband and dual-polarized antennas have received significant attention because of its ability to offer polarization diversity and are being adopted in many multi-functional RF antenna systems to significantly enhance the channel capacity and spectral efficiency, reduce the multipath fading, and maintain reliable wireless communication links.

When designing standalone dual-polarized antenna element for real-world antenna applications, there are multiple electrical and mechanical challenges: 1) the main electrical challenge includes achieving wider impedance bandwidth with stable gain patterns over the operating frequency range, maintaining high orthogonal port isolation and low cross-polarization level to maintain the polarization purity. 2) Besides these electrical challenges, there are also many mechanical and manufacturing challenges such as keeping the antenna profile low with compact size and light weight, ability to manufacture the antennas in large number by leveraging the existing low-cost manufacturing technologies such as the printed circuit board (PCB) manufacturing, and easier integration of the antenna elements with external RF electronics hardware which are extremely important to successfully employ these dual-polarized antenna elements for real-world antenna applications.

Over the past few years, a number of dual-polarized antenna design techniques have been investigated [1], [2], [3], [4], [5], [6], [7], [8], [9], [10], [11], [12], [13], [14], [15], [16], [17], [18], [19], [20], [21]. For example, designing a dual-polarized antenna using Γ-shaped feeding structure is proposed in [1], [2]. However, this method uses a complex feed technique and difficult to manufacture in large quantities, and also, the antennas are high profile in nature. Several stacked patch antennas with probe feed techniques including aperture-coupled feed [6], [7] have been explored. The aperture coupled stacked patch antennas have low cross-polarization level, are easier to integrate with RF electrical hardware, but have backward radiation which reduces the antenna's overall radiation efficiency and gain value. On the other hand, several probe-fed patch antenna design techniques have been reported in literature such as L-shaped

probe [8], meander line probe [10] etc. However, these probe-fed antennas have high cross-polarization level due to the close proximities of the orthogonal ports resulting in polarization impurity. Also, it is inconvenient to connect these antennas with the feed networks in an array environment. A differential driven dual-polarized patch antenna design has been shown in [14] to enhance the orthogonal port isolation and achieve low cross-polarization. However, the differentially driven antennas require balun and differential amplifier to achieve wider impedance bandwidth requiring added hardware and cost. Several magneto-electric dipole antennas in multi-layer stackup were designed for wideband performance [15], [16], [17], [18], [19], [20], [21], [22]. These antennas have the advantage of manufacturing in high-volume using low-cost standard PCB technologies, however, most of these antennas have narrow bandwidth and some use multiple antenna elements to enhance the impedance bandwidth which requires significant amount physical space. In recent years, dipole antennas oriented in orthogonal configuration have gained significant popularity in designing wideband circularly polarized antennas [23], [24], [25], [26], [27], [28], [29], [30], [31], [32], [33], [34], [35], [36]. The crossed-dipole antennas use vacant quarter ring to produce circularly polarized radiation and have the advantage of achieving wide impedance bandwidth and low cross-polarization level; however, these types of antennas have complicated manufacturing and integration techniques and work in single polarization configuration [23], [24], [25], [26], [27], [28], [29], [30], [31], [32], [33], [34], [35], [36] which is a significant challenge to employ them in full-duplex real-world applications.

In this paper, a new way of designing and implementing a standalone dual-polarized and wideband dipole antenna element based on substate-integrated coaxial feed technique is proposed and investigated. To demonstrate the proposed dual-polarized antenna design concept, an antenna structure comprising two sets of planar dipole element in orthogonal configuration and excited by two separate substrate-integrated coaxial feeds is designed and manufactured. By utilizing the substrate-integrated coaxial feed technique, high port-to-port isolation (>20dB) and wider impedance bandwidth (approximately 36%) are achieved. The proposed antenna design method is simple and can easily be manufactured in large quantities by leveraging the existing low-cost printed circuit board (PCB) manufacturing technologies, and also, has easier assembly and integration with the backend RF electronics hardware. This paper is divided into three sections. In Section II, the proposed antenna design method and simulated performance is shown. Section III presents the measurement of a prototype antenna, and a conclusion is drawn in Section IV.

II. ANTENNA DESIGN

A. ANTENNA CONFIGURATION

The proposed antenna configuration is shown in Fig. 1(a). It is a multi-layer structure and has two sets of planar

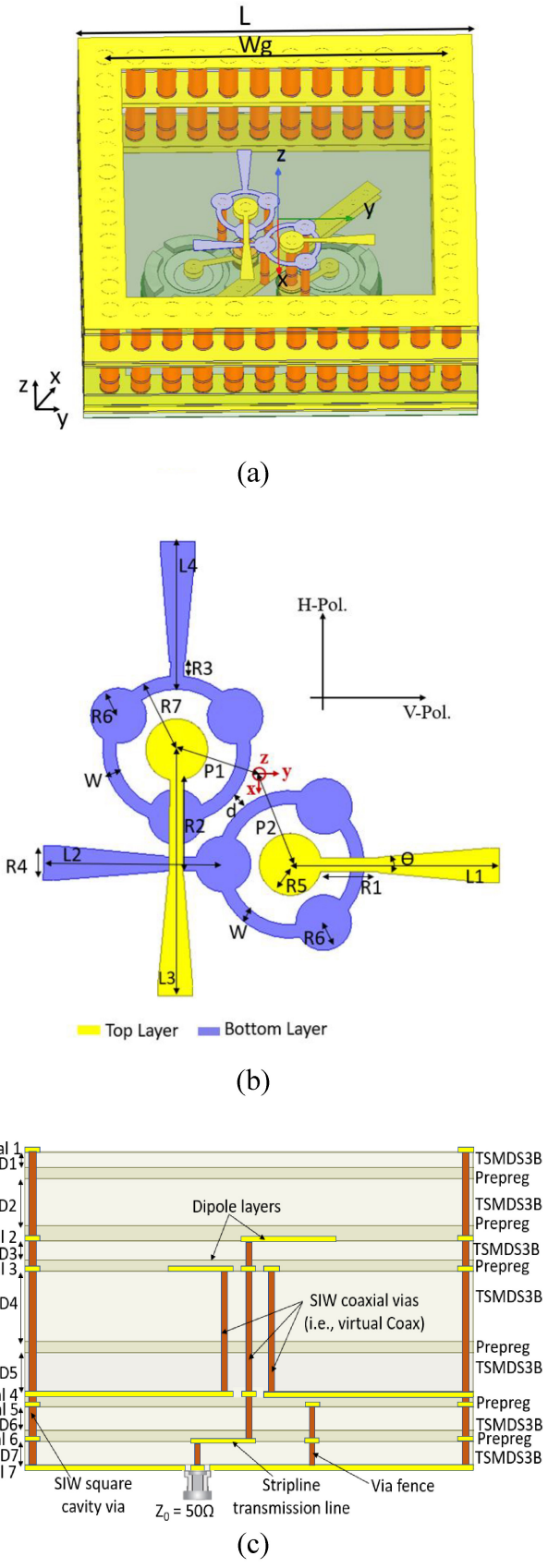

FIGURE 1. Geometry of the proposed antenna structure: a) 3-D view; b) Detailed geometry of the radiating elements; c) Cross-sectional view of the multi-layer stackup.

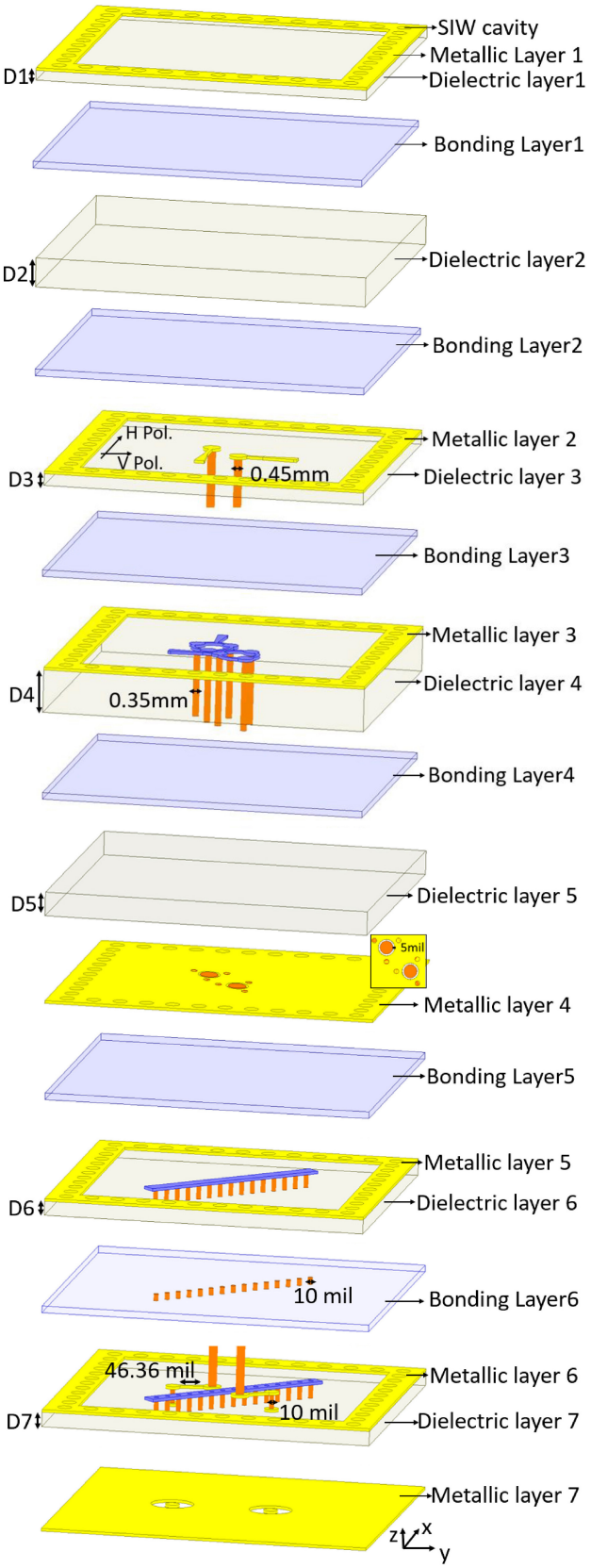

FIGURE 2. Three-dimensional configuration of the overall antenna stackup.

TABLE 1. Antenna dimensions.

R1	R2	R3	R4	R5
34.84mil	57.9mil	8.7mil	21.16mil	18.87mil
R6	R7	L1	L2	L3
16.89mil	40.74mil	126.4mil	108.7mil	149.46mil
L4	Θ	D1	D2	D3
89.8mil	10.075º	10mil	60mil	5 mil
D4	D5	D6	D7	d
60mil	20mil	10mil	10mil	8.4mil
w	L	Wg	P1	P2
8mil	600mil	520mil	52.9mil	52.9mil

modified bowtie-shaped crossed dipole elements printed on the top surfaces of two separate dielectric layers separated by a prepreg bonding layer (Fig. 1(b-c)). To generate orthogonal polarization and maintain high cross-polarization level, the dipole elements are configured in a perpendicular orientation in which the two feed sources exciting the two dipole elements are located in close proximity (Fig. 1(a-b)) resulting in strong port-to-port coupling. To mitigate the port-to-port coupling and improve the orthogonal port isolation, the dipole pairs are excited with two separate substrate-integrated-coaxial feeds (Fig. 1(b-c)). Three plated via holes with a radial via-to-via distance of 70.57mil were embedded in the substrate material to realize the substate integrated coax. Each substrate integrated coax has a radius of 40.57mil which corresponds to a characteristics impedance of 52Ω.

The overall antenna structure is enclosed in a square shaped substrate-integrated waveguide (SIW) cavity to enhance the antenna gain value and minimize the backward radiation. In the SIW cavity, four periodic rows of plated via fence are embedded in the dielectric material to create a square cavity. These plated via rows along with the top and bottom metallic layers (Fig. 1(c)) introduce a structure like a square metallic cavity.

Fig. 1(b-c) and Fig. 2 shows the detailed configuration of the dipole elements and the antenna stackup. The stackup is made up of seven 'TSMDS3B' (dielectric constant $\varepsilon_r = 2.95$, loss tangent $\delta = 0.0011$) dielectric materials of different thicknesses (Fig. 1(c) & Fig. 2) with six 4mil-thick 'RO4550' (dielectric constant $\varepsilon_r = 3.52$, loss tangent $\delta = 0.004$) prepreg bonding layers and seven 0.5oz copper layers. To prevent possible electrical shorting during the electroplating and lamination process, several non-functional via pads were implemented on the anti-pad layers (Fig. 1(c)). The two dipole elements of the antenna structure (Fig. 1) are excited through two sub miniature push-on micro (SMPM) RF connectors. The two feed vias of the proposed dual polarized antenna structure are located in close proximity which complicates the connector assembly due to narrower

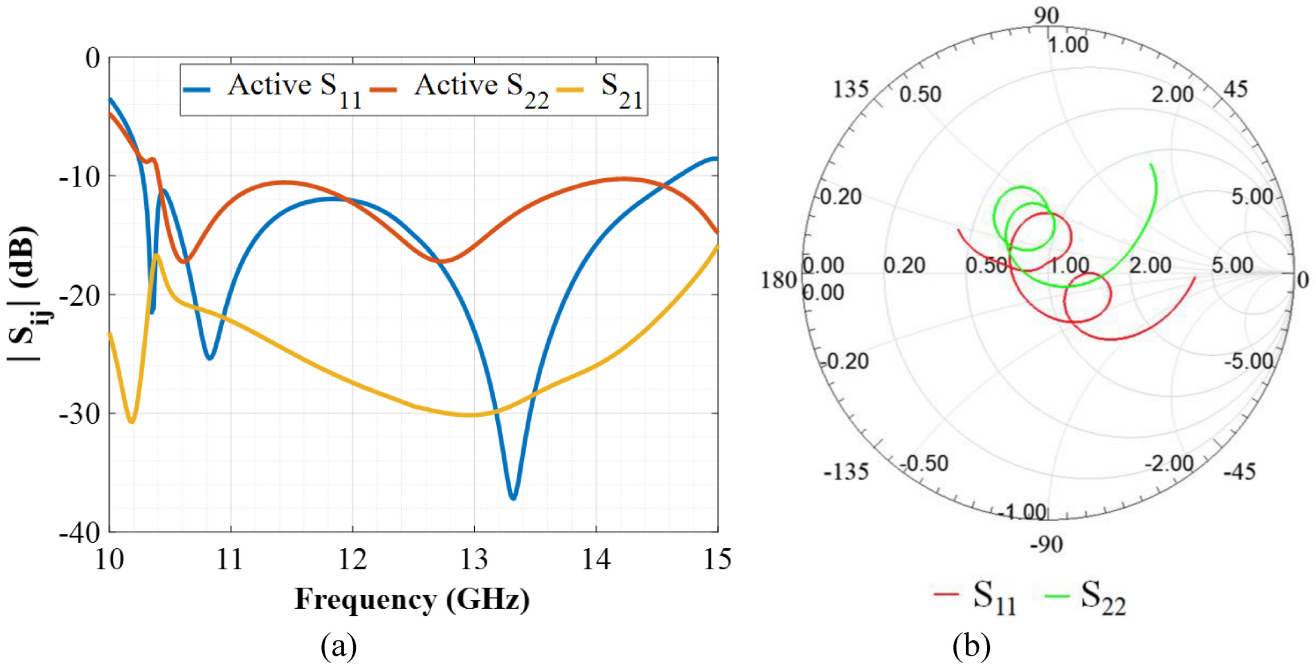

FIGURE 3. (a) Simulated active reflection coefficients (active $|S_{11}|$ & active $|S_{22}|$) and port-to-port isolation ($|S_{21}|$); (b) S_{11} & S_{22} Smith chart.

spacing between the two feed vias of the antenna structure. To facilitate the connector integration, a stripline layer with two extended transmission lines is implemented underneath the antenna ground plane. The stripline layer includes a via fence (Fig. 1(c) & Fig. 2) between the two-transmission lines to mitigate the interference between the two orthogonally polarized electric field lines. By adjusting the length of the two transmission lines, the relative spacing between the two antenna ports can be made flexible to accommodate the RF connectors and ease the external RF electronics hardware integration.

B. SIMULATION RESULTS

The proposed antenna structure was designed and simulated using Ansys' electromagnetic solver High Frequency Structural Simulator (HFSS) version 2022R1 software package. All the design parameters including the via diameters, minimum via-to-via distance (10mil) and via pads were optimized to meet the printed circuit board (PCB) manufacturer's design guidelines and Table 1 presents the dimensions of the different parameters of the designed antenna structure. Fig. 3a demonstrates the simulated active reflection coefficients (active $S_{ii} = S_{ii} + \sum_{i \neq j} S_{ij}$) and the port-to-port isolation ($|S_{21}|$) between the two orthogonally polarized antenna ports. Fig. 3b shows the Smith chart of simulated S_{11} and S_{22}. From the simulated predictions, it is obvious that the designed antenna structure has a relatively wide impedance bandwidth with the $|S_{11}|$ and $|S_{22}|$ less than -10dB over 10.28-14.78GHz frequency band and the port-to-port coupling ($|S_{21}|$) is less than -20dB across most of the frequency band. The fractional impedance bandwidth is about 36%.

To predict the radiation patterns and calculate the cross-polarization, the designed antenna structure was simulated in both dual-linear (Vertical/Horizontal) polarization and dual-circular (Right-hand/Left-hand) polarization configurations, and the antenna gain patterns in both configurations were predicted in HFSS. For the configuration of dual linear polarization, one antenna port (vertical or horizontal) was excited at a time and the other port was terminated with a 50Ω resistive load. For dual circular-polarization configuration, both the antenna ports were excited simultaneously with a 90° phase difference between the two orthogonal ports. Fig. 4(a-d) shows the simulated two-dimensional antenna radiation patterns along the XZ and YZ planes at 10.7GHz and 13.75GHz for dual linear polarization configuration and Fig. 4(e-f) shows the radiation patterns for dual circular polarization configuration at 10.7GHz and 13.75GHz. The simulated radiation pattens at 12.5GHz is shown in Fig. 5(a) as a function of the elevation angle and Fig. 5(b) presents the co-pol and cross-pol broadside peak gain patterns as a function of frequency. From the simulated predictions, it is observed that the designed antenna has a 16dB lower cross-pol. gain level over most of the frequency band.

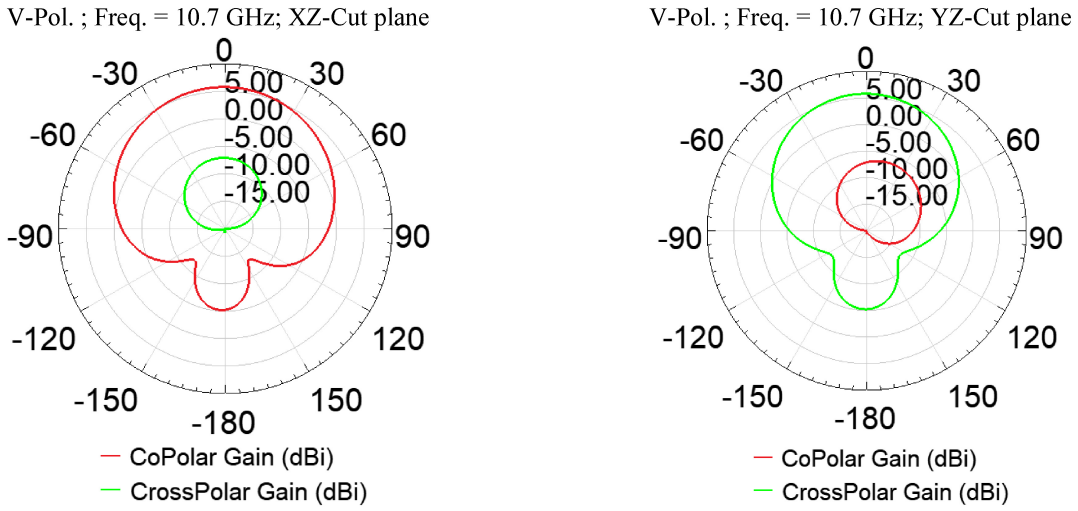

(a)

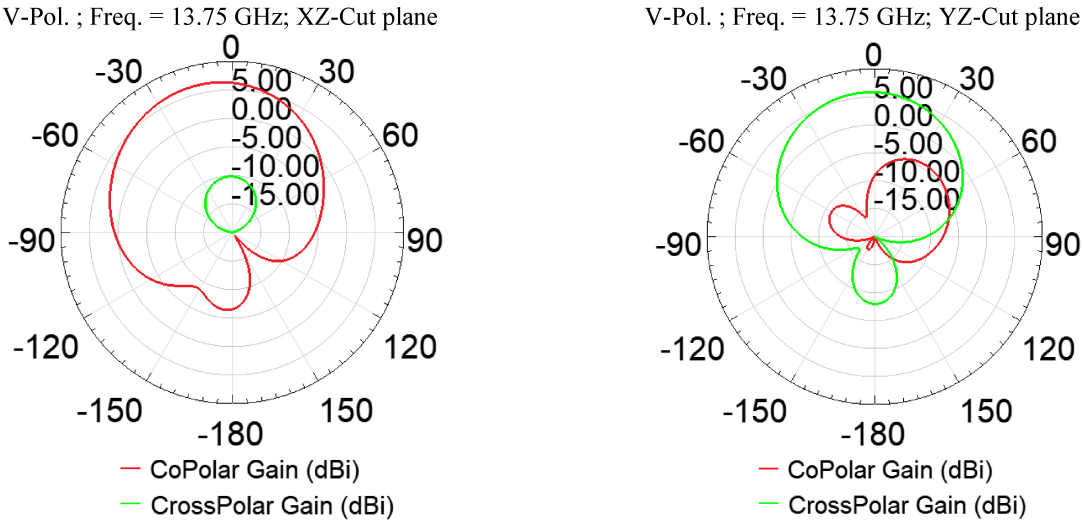

(b)

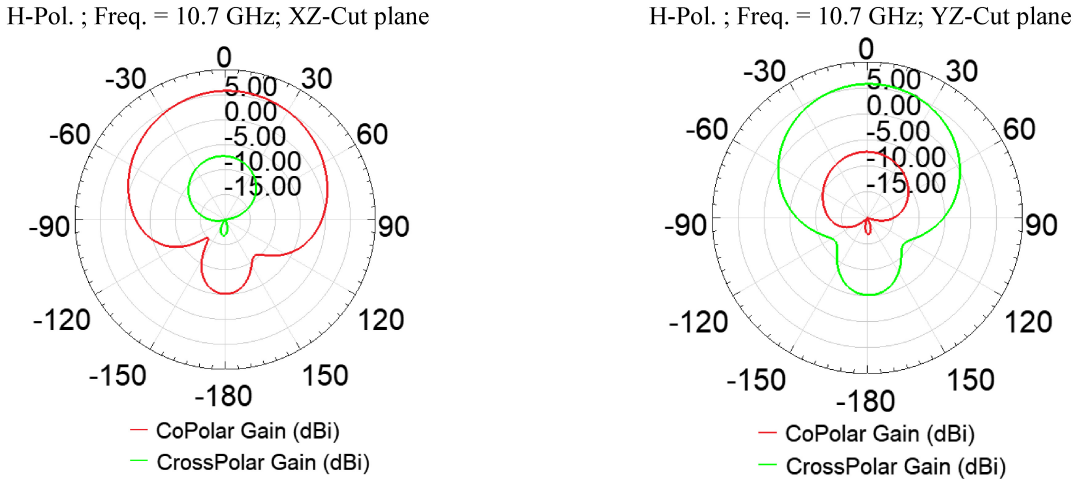

(c)

FIGURE 4. Simulated two-dimensional co-pol/cross-pol radiation patterns along the xz-plane (left) and yz-plane (right) at: (a) 10.7GHz (V-Pol. = ON, H-Pol. = 50Ω Loaded), (b) 13.75GHz (V-Pol. = ON, H-Pol. = 50Ω Loaded), (c) 10.7GHz (V-Pol. = 50Ω Loaded, H-Pol. = ON).

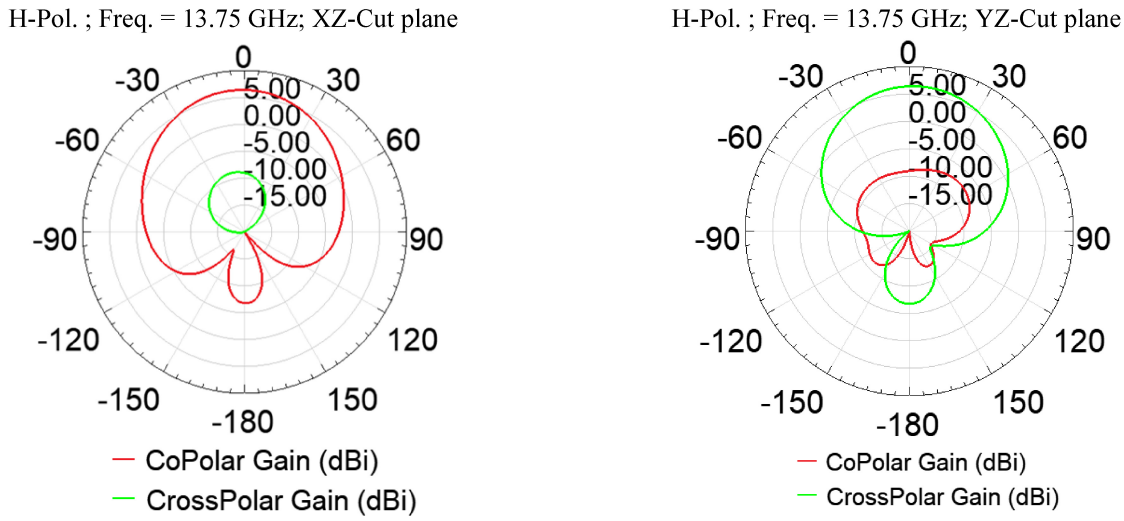

(d)

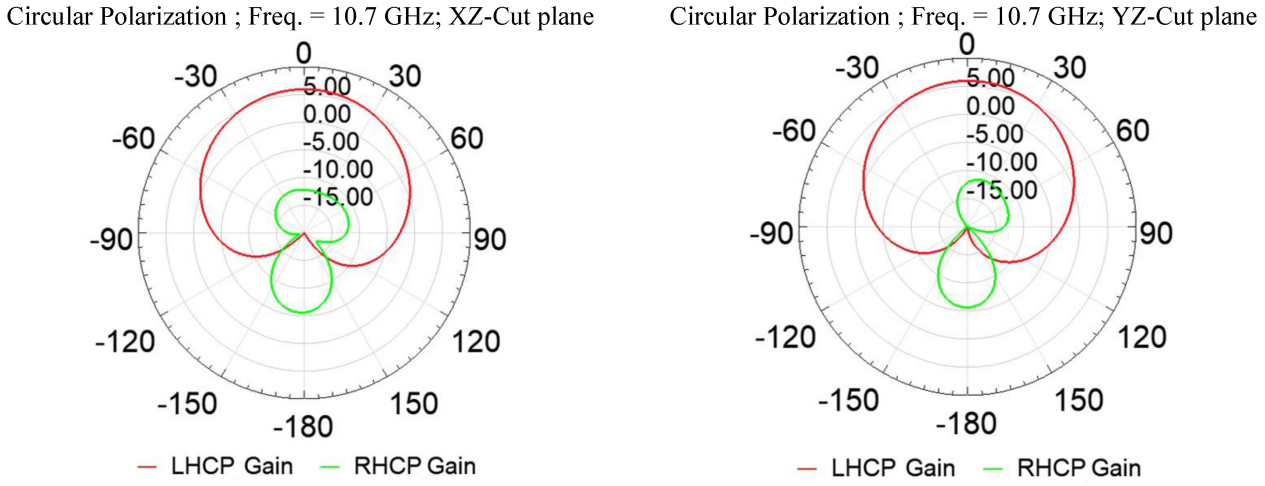

(e)

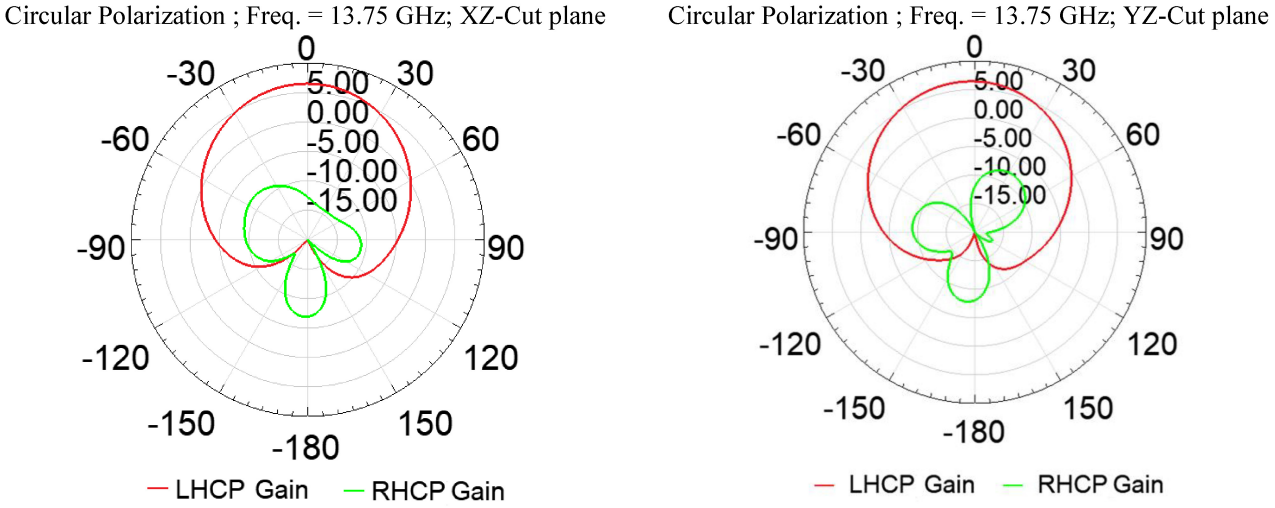

(f)

FIGURE 4. ***(Continued.)*** **Simulated two-dimensional co-pol/cross-pol radiation patterns along the xz-plane (left) and yz-plane (right) at: (d) 13.75GHz (V-Pol. = 50Ω Loaded, H-Pol. = ON), (e) 10.7GHz (V-Pol. = ON, H-Pol. = ON; with 90° phase difference), (f) 13.75GHz (V-Pol. = ON, H-Pol. = ON; with 90° phase difference).**

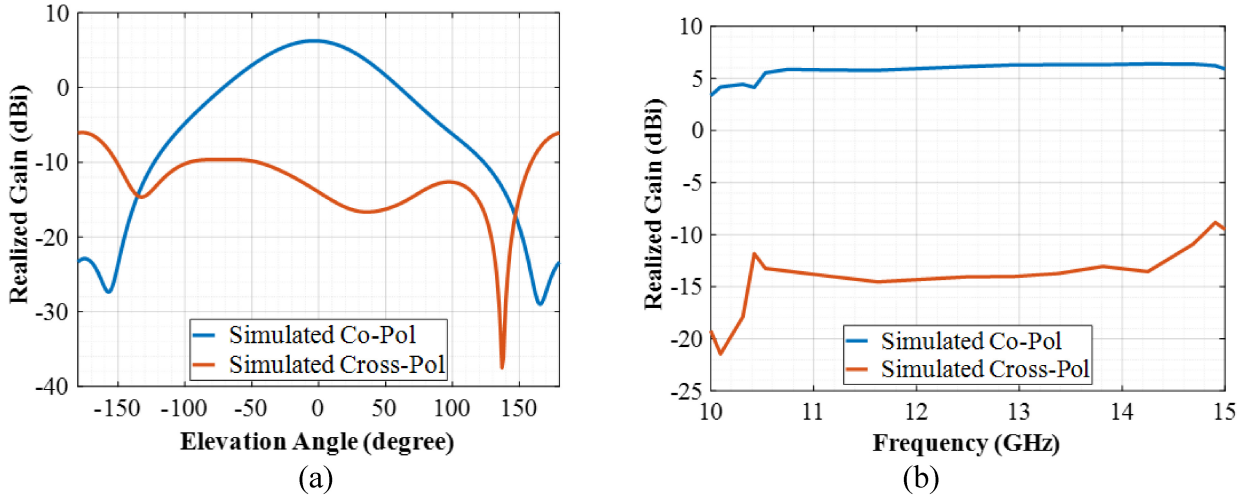

FIGURE 5. (a) Simulated Co-pol and Cross-Pol radiation patterns at 12. 5GHz as a function of elevation angle; (b) Simulated Co-Pol and Cross-Pol broadside gain patterns as a function of frequency.

C. PHASE CENTER OF THE DUAL-POLARIZED DIPOLE ELEMENTS

The two orthogonally polarized dipole elements (i.e., the vertical and horizontal dipoles) in the proposed antenna structure are positioned slightly offset (by 52.9mil) relative to the center of the antenna structure to accommodate the substrate integrated coaxial via fences and this results in a phase center offset between the horizontal and vertically polarized dipole elements. For the proposed dual-polarized antenna structure to be useful for practical applications, it is necessary to evaluate the effect of the phase center offset on the antenna polarization purity over the operating frequency range. The phase center of an antenna is a point at which the far field emanates, i.e., all the electromagnetic field waves radiated from the antenna elements have equal phase front along the spherical curvature at that imaginary point [37], [38], [39].

To calculate the phase center variations of the designed antenna structure using HFSS software, the radiation boundary of the designed antenna structure was moved in along the z-axis and the phase variation over the beamwidth was minimized using HFSS. Fig. 6(a) shows the simulated phase center variations of the two linearly polarized antenna element as a function of the scan angle at 11GHz. As seen, the phase offset between the H-pol. and V-pol. dipoles is relatively smaller (9°) along the boresight and has little effect on the axial ratio performance at the operating frequency range. Fig. 6(b) presents the simulated phase center variation over the frequency range. As evident, the phase center variation of the two orthogonal dipole elements is relatively stable over the entire operating frequency range.

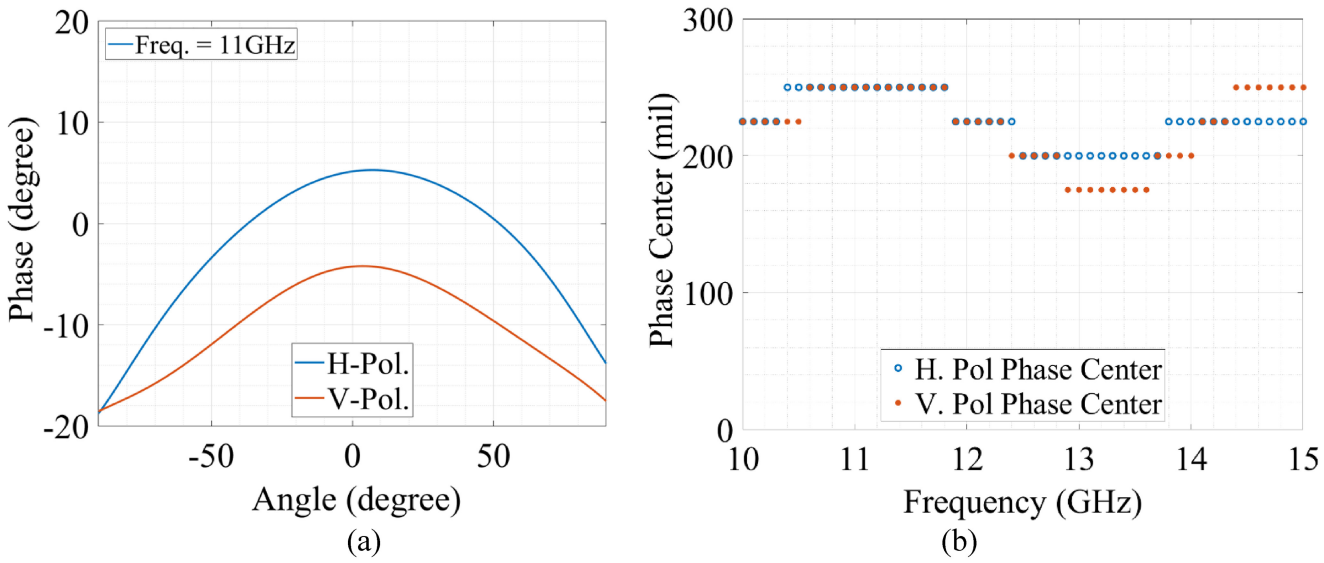

FIGURE 6. Simulated phase center variation of the two linearly polarized dipole elements: (a) V-Pol. and H-Pol. phase center variation with the elevation angle; (b) Phase center variation as a function of frequency.

III. MEASUREMENT AND VALIDATION

A prototype of the designed multi-layer antenna structure was manufactured using standard printed circuit board (PCB) manufacturing technique and assembled with two surface mounted standard sub miniature push-on micro (SMPM) connectors at the two excitation ports. Fig. 7 shows a picture of the fabricated antenna prototype. A 4-port vector network analyzer (Rhode and Schwarz's ZNB40) was used for measuring the reflection/transmission coefficients and the far-field radiation patterns. The measured antenna gain of the fabricated antenna, in both linear/circular polarization configuration, was calculated by comparing with a Ku-band standard gain horn antenna. To calculate the circularly polarized gain patterns, a COTS 90° hybrid coupler was used to generate the 90° phase difference between the two orthogonal (vertical/horizontal) antenna ports.

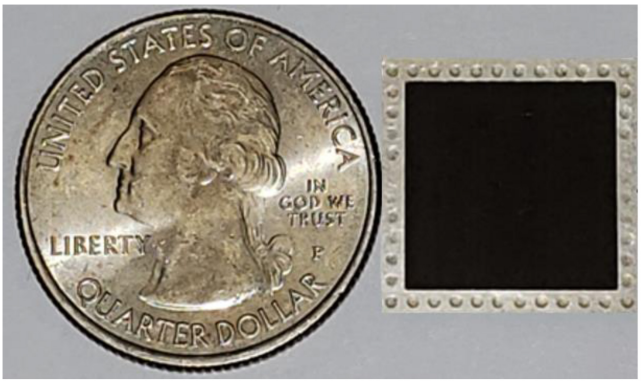

FIGURE 7. Fabricated antenna prototype.

A. MEASURED RESULTS IN DUAL LINEAR POLARIZATION CONFIGURATIONS

The measured results of the reflection coefficients and port-to-port isolation are shown in Fig. 8 (a-b) and compared with the simulated predictions. From the comparison, it is seen that the measurements agree well with the HFSS simulations. The simulated impedance bandwidth for $|S_{ii}|$ lower than -10dB is 36% (10.28-14.8GHz) while the measured $|S_{ii}|$ is less than -10dB from 9.9GHz to 14.5GHz, corresponding to a fractional bandwidth of 37.7%. The measured port-to-port isolation is greater than 20dB at most frequencies over 9.7-14.7GHz frequency range.

To measure the radiation patterns in dual linear polarization configuration, the vertical and horizontally polarized antenna elements were excited at a time while the other one was terminated with a 50Ω load. To calculate the gain patterns as a function of angle and frequency, the testing antenna was rotated under computer control and on the receive end, a standard gain horn antenna was used and oriented in vertical and horizontal configuration to calculate the co-pol/cross-pol gain patterns of the testing antenna. Radar absorbing materials was placed all around to reduce any wanted reflections. The measured and simulated co-pol/cross-pol gain patterns of the fabricated antenna at 12.5GHz and 13.5GHz are shown in Fig. 9 for vertical/horizontal polarization and Fig. 10 presents the gain patterns as a function of frequency. As seen, the gain patterns are relatively stable and symmetric around the broadside peak gain, and the cross-polarization levels are approximately 16dB lower than the broadside peak gains. The smaller deviations and ripples in the measured results can be attributed to the reflections and losses in the RF cables, connectors, attenuators, and the fabrication tolerances.

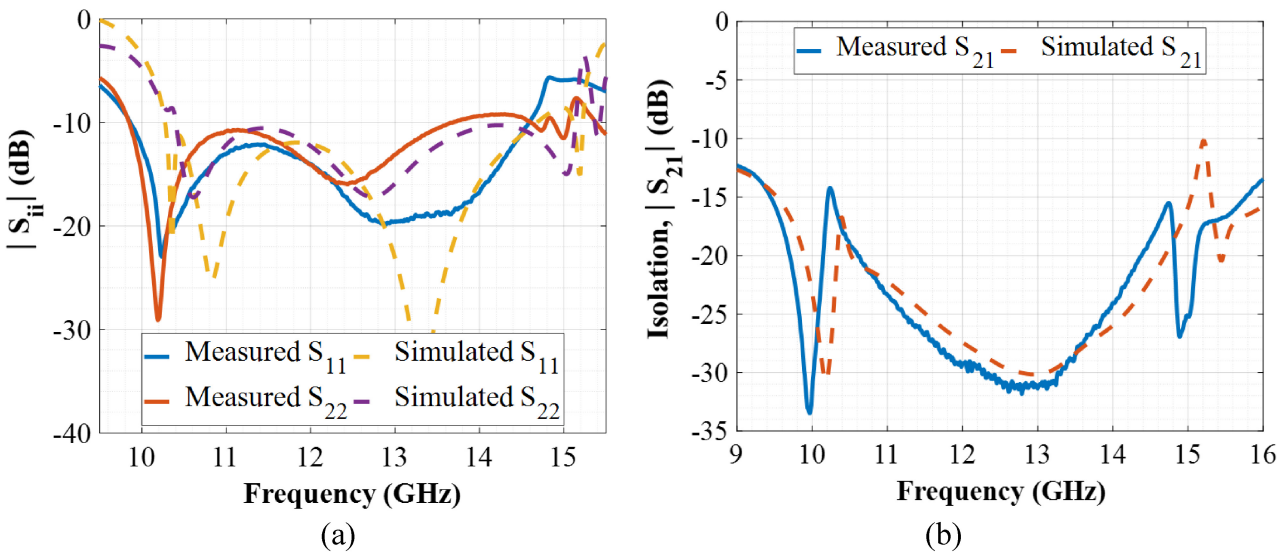

FIGURE 8. (a) Comparison of measured and simulated return losses ($|S_{11}|$ & $|S_{22}|$); and (b) Measured and simulated port-to-port isolation ($|S_{21}|$.

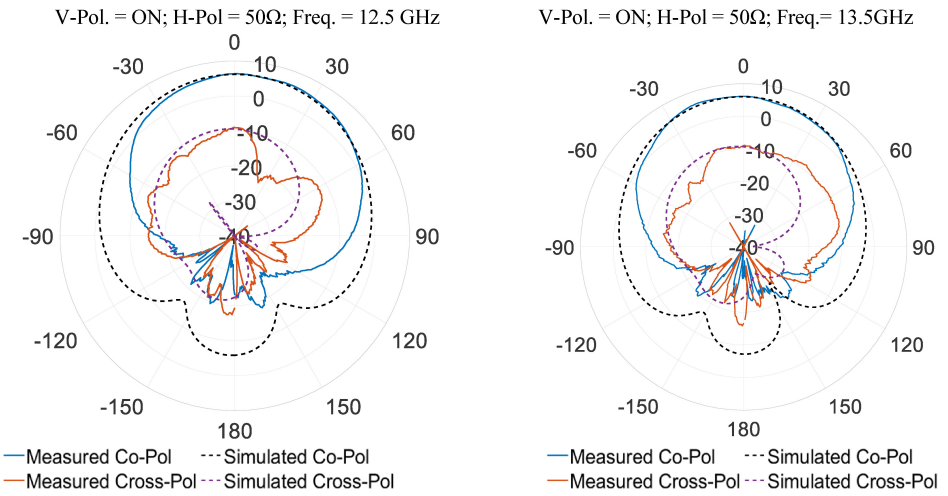

(a)

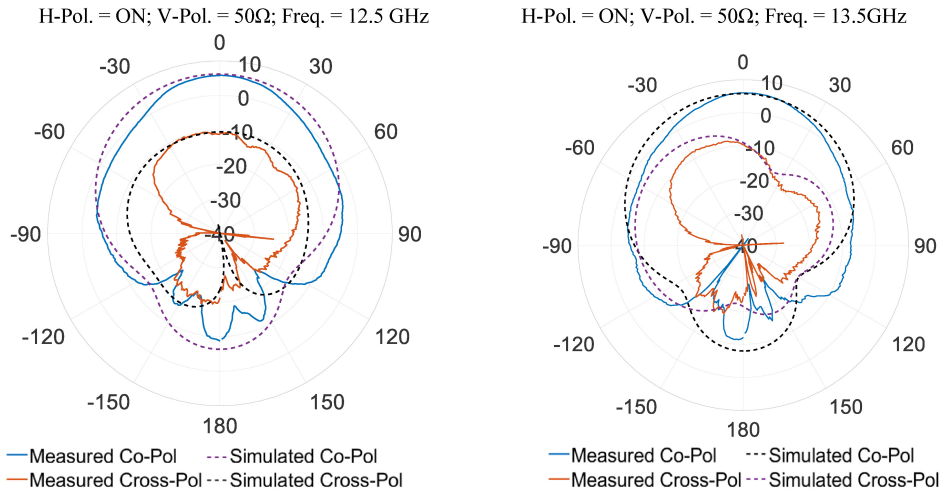

(b)

FIGURE 9. Measured co- and cross-polarized radiation patterns at 12.5GHz and 13.5GHz of the designed antenna and comparison with simulated prediction: (a) V-Pol. is excited, and H-Pol. is terminated with 50Ω load (YZ-plane); (b) H-Pol. is excited and V-Pol. is terminated with 50Ω load (XZ-plane).

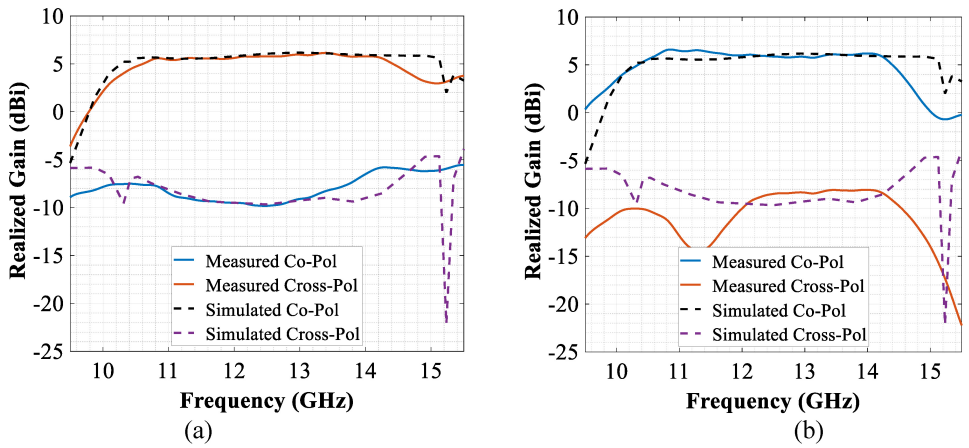

FIGURE 10. Measured and simulated co-pol. and cross-pol. gain patterns as a function of frequency: a) V-Pol. is excited, and H-Pol. is terminated with 50Ω load; (b) H-Pol. is excited and V-Pol. is terminated with 50Ω load.

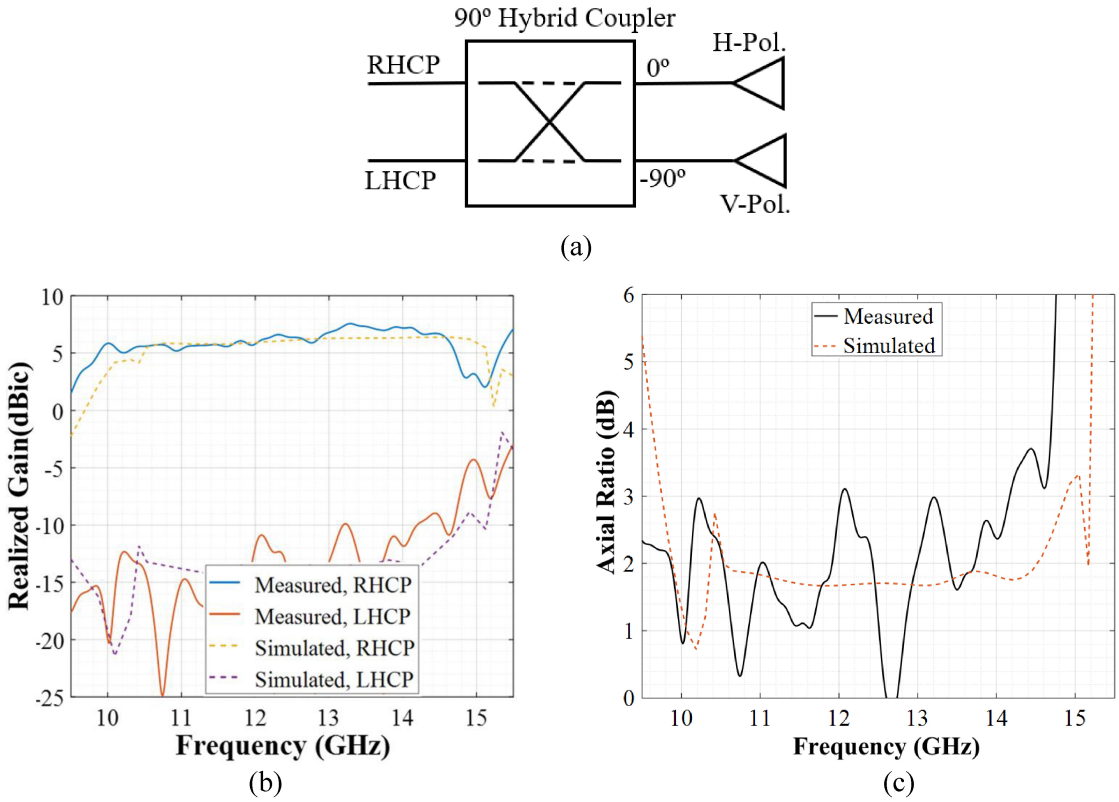

FIGURE 11. (a) Schematic of the dual linearly polarized antenna ports with 90° hybrid coupler; (b) Comparison of measured and simulated RHCP/LHCP gain patterns as a function of frequency; (c) Measured and simulated axial ratios.

TABLE 2. Comparison of similar PCB-based dual-polarized antennas.

Ref.	No. of Antenna Elements	Manufacturing Technology	Feed Network	Impedance BW**	Port-to-Port Isolation	Cross Pol. Separation
[15]	4x4 array	LTCC	Microstrip to SIW transition	45%	>14dB	<15dB
[16]	2x2 array	PCB	Microstrip line	50%	>17dB	12dB
[17]	1x4 array	PCB	Microstrip line	26.3%	20dB	<15dB
[18]	1x4 array	PCB	Meandered via	47%	20dB	16dB
[19]	2x2 array	PCB	4-way corporate feed	19.8%	35dB	33dB
[20]	Single element	PCB	Slots and extended feedline	27.6%	30dB	20dB
[21]	Single element	PCB	Microstrip to Ridge gap waveguide transition	23.4%	20dB	20dB
[22]	Single element	PCB	Two pins feeding technique	28.4%	-	-
This Work	Single element	PCB	SIW Coax.	36%	>20dB	<16dB

**Impedance BW% refers to the measured impedance bandwidth with $|S11| < -10$ dB or VSWR < 2.

B. MEASURED RESULTS IN DUAL CIRCULAR POLARIZATION CONFIGURATIONS

To generate right-hand and left-hand circular polarization (RHCP and LHCP) from the proposed dual linearly polarized antenna structure, a COTS 90° hybrid coupler was connected to the two linearly polarized antenna ports (i.e., H/V ports) to generate a 90° phase difference between the two orthogonal dipole elements as shown in Fig. 11(a) [40], and the axial ratio performance and RHCP/LHCP gain patterns were measured. Fig. 11(b-c) compares the measured and simulated co-pol/cross-pol (i.e., RHCP/LHCP) gain patterns and the corresponding axial ratio as a function of frequency. The designed antenna with the 90° hybrid coupler exhibits a wide axial ratio bandwidth and the 3dB axial ratio bandwidth is about 34.5%.

Table 2 compares the performance characteristics of the proposed dual-polarized crossed-dipole antenna structure with other PCB-based dual-polarized antennas. It is

evident that the proposed standalone dual-linearly polarized antenna achieves relatively wide impedance bandwidth with low cross-polarization level and high port-to-port isolation.

IV. CONCLUSION

In this paper, a new way of designing and implementing a wideband and dual-polarized standalone antenna element has been demonstrated. The antenna design method is straightforward and employs two sets of substrate-integrated coaxial feeds to improve the orthogonal port isolation between the two antenna ports. Measured results show that the proposed antenna has a relatively wider impedance bandwidth (about 36%), high orthogonal port isolation (>20dB), and low cross polarization level (lower than 16dB). The radiation patterns are relatively stable and symmetric over the operating frequency range. The proposed antenna structure is mechanically robust and has planar configuration which makes it easily integrable with the external RF electronics hardware without having any integration issues and cable requirement. Also, the proposed multi-layer antenna structure can easily be manufactured in high-volume by leveraging existing low-cost PCB manufacturing technologies.

REFERENCES

[1] B. Q. Wu and K.-M. Luk, "A broadband dual-polarized magneto-electric dipole antenna," *IEEE Antennas Wireless Propag. Lett.*, vol. 8, pp. 60–63, 2009.

[2] D.-L. Wen and Q.-X. Chu, "A broadband dual-polarized antenna with Γ-shaped feeding structures," in *Proc. 9th Eur. Conf. Antennas Propag.*, 2015, pp. 1–4.

[3] B. Li, Y. Yin, W. Hu, Y. Ding, and Y. Zhao, "Wideband dual-polarized patch antenna with low cross polarization and high isolation," *IEEE Antennas Wireless Propag. Lett.*, vol. 11, pp. 427–430, 2012.

[4] W. Qiu, C. Chen, H. Zhang, and W. Chen, "A wideband dual-polarized L-probe antenna array with hollow structure and modified ground plane for isolation enhancement," *IEEE Antennas Wireless Propag. Lett.*, vol. 16, pp. 2820–2823, 2017.

[5] S. Zhou, P. Tan, and T. Chio, "Low-profile, wideband dual-polarized antenna with high isolation and low cross polarization," *IEEE Antennas Wireless Propag. Lett.*, vol. 11, pp. 1032–1035, 2012.

[6] S. D. Targonski, R. B. Waterhouse, and D. M. Pozar, "Design of wide-band aperture-stacked patch microstrip antennas," *IEEE Trans. Antennas Propag.*, vol. 46, no. 9, pp. 1245–1251, Sep. 1998.

[7] K. Ghorbani and R. B. Waterhouse, "Dual polarized wide-band aperture stacked patch antennas," *IEEE Trans. Antennas Propag.*, vol. 52, no. 8, pp. 2171–2175, Aug. 2004.

[8] H. Wong, K.-L. Lau, and K.-M. Luk, "Design of dual-polarized L-probe patch antenna arrays with high isolation," *IEEE Trans. Antennas Propag.*, vol. 52, no. 1, pp. 45–52, Jan. 2004.

[9] Y. X. Guo, K. W. Khoo, and L. C. Ong, "Wideband dual-polarized patch antenna with broadband baluns," *IEEE Trans. Antennas Propag.*, vol. 55, no. 1, pp. 78–83, Jan. 2007.

[10] H. W. Lai and K. M. Luk, "Dual polarized patch antenna fed by meandering probes," *IEEE Trans. Antennas Propag.*, vol. 55, no. 9, pp. 2625–2627, Sep. 2007.

[11] K. S. Ryu and A. A. Kishk, "Wideband dual-polarized microstrip patch excited by hook shaped probe," *IEEE Trans. Antennas Propag.*, vol. 56, no. 12, pp. 3645–3649, Dec. 2008.

[12] J. Huang, Z. A. Hussein, and A. Petros, "A VHF microstrip antenna with wide-bandwidth and dual-polarization for sea ice thickness measurement," *IEEE Trans. Antennas Propag.*, vol. 55, no. 10, pp. 2718–2722, Oct. 2007.

[13] J. L. Vazquez-Roy, V. Krozer, and J. Dall, "Wideband dual-polarization microstrip patch antenna array for airborne ice sounder," *IEEE Antennas Propag. Mag.*, vol. 54, no. 4, pp. 98–107, Aug. 2012.

[14] L.-H. Wen, S. Gao, Q. Luo, Q. Yang, W. Hu, and Y. Yin, "A low-cost differentially driven dual-polarized patch antenna by using open-loop resonators," *IEEE Trans. Antennas Propag.*, vol. 67, no. 4, pp. 2745–2750, Apr. 2019.

[15] Y. Li, C. Wang, and Y. X. Guo, "A Ka-band wideband dual-polarized magnetoelectric dipole antenna array on LTCC," *IEEE Trans. Antennas Propag.*, vol. 68, no. 6, pp. 4985–4990, Jun. 2020.

[16] X. Dai and K. M. Luk, "A wideband dual-polarized antenna for millimeter-wave applications," *IEEE Trans. Antennas Propag.*, vol. 69, no. 4, pp. 2380–2385, Apr. 2021.

[17] Y.-W. Hsu, T.-C. Huang, H.-S. Lin, and Y.-C. Lin, "Dual-polarized quasi Yagi–Uda antennas with endfire radiation for millimeter-wave MIMO terminals," *IEEE Trans. Antennas Propag.*, vol. 65, no. 12, pp. 6282–6289, Dec. 2017.

[18] Y. C. Chang, C. C. Hsu, M. I. Magray, H. Y. Chang, and J.-H. Tarng, "A novel dual-polarized wideband and miniaturized low profile magneto-electric dipole antenna array for mmWave 5G applications," *IEEE Open J. Antennas Propag.*, vol. 2, pp. 326–334, 2021.

[19] W. Wei, W. Jing, L. Aimeng, and G. Meng, "Design of 2 by 2 dual-polarized antenna array with high isolation, wideband and low cross polarization," in *Proc. IEEE Int. Symp. Antennas Propag. USNC/URSI Nat. Radio Sci. Meeting*, 2017, pp. 2161–2162.

[20] S. J. Yang, Y. M. Pan, Y. Zhang, Y. Gao, and X. Y. Zhang, "Lowprofile dual-polarized filtering magneto-electric dipole antenna for 5G applications," *IEEE Trans. Antennas Propag.*, vol. 67, no. 10, pp. 6235–6243, Oct. 2019.

[21] M. M. M. Ali, I. Afifi, and A.-R. Sebak, "A dual-polarized magneto-electric dipole antenna based on printed ridge gap waveguide technology," *IEEE Trans. Antennas Propag.*, vol. 68, no. 11, pp. 7589–7594, Nov. 2020.

[22] A. Kumar and S. Raghavan, "Broadband dual-circularly polarized SIW cavity antenna using a stacked structure," *IET Electron. Lett.*, vol. 53, no. 17, pp. 1171–1172, Aug. 2017.

[23] J.-W. Baik, K.-J. Lee, W.-S. Yoon, T.-H. Lee, and Y.-S. Kim, "Circularly polarised printed crossed dipole antennas with broadband axial ratio," *Electron. Lett.*, vol. 44, no. 13, pp. 785–786, Jun. 2008.

[24] K. Saurav, D. Sarkar, A. Singh, and K. V. Srivastava, "Multiband circularly polarized cavity-backed crossed dipole antenna," *IEEE Trans. Antennas Propag.*, vol. 63, no. 10, pp. 4286–4296, Oct. 2015.

[25] J.-W. Baik, T.-H. Lee, S. Pyo, S.-M. Han, J. Jeong, and Y.-S. Kim, "Broadband circularly polarized crossed dipole with parasitic loop resonators and its arrays," *IEEE Trans. Antennas Propag.*, vol. 59, no. 1, pp. 80–88, Jan. 2011.

[26] Y. Feng, J. Li, B. Cao, J. Liu, G. Yang, and D.-J. Wei, "Cavity-backed broadband circularly polarized cross-dipole antenna," *IEEE Antennas Wireless Propag. Lett.*, vol. 18, no. 12, pp. 2681–2685, Dec. 2019.

[27] S. X. Ta, J. J. Han, and I. Park, "Compact circularly polarized composite cavity-backed crossed dipole for GPS applications," *J. Electromagn. Eng. Sci.*, vol. 13, no. 1, pp. 44–49, Mar. 2013.

[28] S. X. Ta, H. Choo, I. Park, and R. W. Ziolkowski, "Multi-band, wide-beam, circularly polarized, crossed, asymmetrically barbed dipole antennas for GPS applications," *IEEE Trans. Antennas Propag.*, vol. 61, no. 11, pp. 5771–5775, Nov. 2013.

[29] G. Feng, L. Chen, X. Wang, X. Xue, and X. Shi, "Broadband circularly polarized crossed bowtie dipole antenna loaded with parasitic elements," *IEEE Antennas Wireless Propag. Lett.*, vol. 17, no. 1, pp. 114–117, Jan. 2018.

[30] T. K. Nguyen, H. H. Tran, and N. Nguyen-Trong, "A wideband dual-cavity-backed circularly polarized crossed dipole antenna," *IEEE Antennas Wireless Propag. Lett.*, vol. 16, pp. 3135–3138, 2017.

[31] W.-J. Yang, Y.-M. Pan, and S.-Y. Zheng, "A compact broadband circularly polarized crossed-dipole antenna with a very low profile," *IEEE Antennas Propag. Lett.*, vol. 18, no. 10, pp. 2130–2134, Oct. 2019.

[32] R. Xu, J. Li, and W. Kun, "A broadband circularly polarized crossed-dipole antenna," *IEEE Trans. Antennas Propag.*, vol. 64, no. 10, pp. 4509–4513, Oct. 2016.
[33] H. H. Tran and I. Park, "Wideband circularly polarized cavity-backed asymmetric crossed bowtie dipole antenna," *IEEE Antennas Wireless Propag. Lett.*, vol. 15, pp. 358–361, 2016.
[34] Y. He, W. He, and H. Wong, "A wideband circularly polarized cross-dipole antenna," *IEEE Antennas Wireless Propag. Lett.*, vol. 13, pp. 67–70, 2014.
[35] J. Fan, J. Lin, J. Cai, and F. Qin, "Ultra-wideband circularly polarized cavity-backed crossed-dipole antenna," *Sci. Rep.*, vol. 12, p. 4569, Mar. 2022.
[36] W. Yang, Y. Pan, S. Zheng, and P. Hu, "A low-profile wideband circularly polarized crossed-dipole antenna," *IEEE Antennas Wireless Propag. Lett.*, vol. 16, pp. 2126–2129, 2017.
[37] *IEEE Standard for Definitions of Terms for Antennas*, IEEE Standard 145-2013, 2013.
[38] K. Harima, M. Sakasai, and K. Fujii, "Determination of gain for pyramidal-horn antenna on basis of phase center location," in *Proc. IEEE Int. Symp. Electromagn. Compat.*, 2008, pp. 1–5.
[39] E. L. Holzman, "A comparison of dual-polarized, periodic arrays of coincident and noncoincident phase center radiators," *IEEE Trans. Antennas Propag.*, vol. 61, no. 3, pp. 1471–1474, Mar. 2013.
[40] D. M. Pozar, *Microwave Engineering*, 4th ed. Hoboken, NJ, USA: Wiley, 2005, pp. 343–346.

SOUMITRA BISWAS (Senior Member, IEEE) received the Ph.D. degree in electrical engineering from the University of Delaware, Newark, DE, USA, in 2019. His research interests include phased array antennas, graded-index (GRIN) lens antennas, wideband and dual-polarized printed circuit board antennas, and integrated RF and microwave subsystems.